◆ Human Brain Mapping 14:108–115(2001) ◆

Influence of EEG Electrodes on the BOLD fMRI Signal

Giorgio Bonmassar,[1]* Nouchine Hadjikhani,[1] John R. Ives,[2] Denise Hinton,[1] and John W. Belliveau[1]

[1]*A. Martinos Center, Massachusetts General Hospital, Charlestown, Massachusetts*
[2]*Neurology Department, Beth Israel Deaconess Medical Center, Boston, Massachusetts*

Abstract: Measurement of the EEG during fMRI scanning can give rise to image distortions due to magnetic susceptibility, eddy currents or chemical shift artifacts caused by certain types of EEG electrodes, cream, leads, or amplifiers. Two different creams were tested using MRS and T2* measurements, and we found that the one with higher water content was superior. This study introduces an index that quantifies the influence of EEG equipment on the BOLD fMRI signal. This index can also be used more generally to measure the changes in the fMRI signal due to the presence of any type of device inside (or outside) of the field of view (e.g., with fMRI and diffuse optical tomography, infrared imaging, transcranial magnetic stimulation, ultrasound imaging, etc.). Quantitative noise measurements are hampered by the normal variability of functional activation within the same subject and by the different slice profiles obtained when inserting a subject multiple times inside a MR imaging system. Our measurements account for these problems by using a matched filtering of cortical surface maps of functional activations. The results demonstrate that the BOLD signal is not influenced by the presence of EEG electrodes when using a properly constructed MRI compatible recording cap. *Hum. Brain Mapping 14:108–115, 2001.*

Key words: electroencephalography; functional magnetic resonance imaging; MRI; MRI artifacts; magnetic susceptibility; eddy currents; chemical shifts

INTRODUCTION

The measurement of EEG during fMRI is a new tool in epilepsy research [Chiappa et al., 1999; Hill et al., 1999; Huang-Hellinger et al., 1995; Ives et al., 1993; Krakow et al., 1999; Schomer et al., 2000; Seeck et al., 1998; Symms et al., 1999; Warach et al., 1996]. As this technique becomes increasingly popular, the need for evaluating possible image artifacts on the fMRI BOLD signal arises [Krakow et al., 2000].

Image artifacts in simultaneous EEG/fMRI measurements can arise due to the presence of EEG paste, electrodes, and leads inside the field of view (FOV). Typically, susceptibility artifacts create magnetic field inhomogeneities and interfere with the gradient fields used in MR imaging. Susceptibility artifacts can be greatly diminished by the use of non-ferromagnetic metals or alloys [Lufkin et al., 1988; New et al., 1983]. In this study, we used conductive-plastic electrodes [Bonmassar et al., 1999; Ives et al., 1998] coated with a thin layer of silver epoxy to achieve both high quality

Contract grant sponsor: Whitaker Foundation; Contract grant sponsor: National Institutes of Health and National Foundation for Functional Brain Imaging; Contract grant number: RO1 NS37462, P41 RR14075.

*Correspondence to: Giorgio Bonmassar, A. Martinos Center, Massachusetts General Hospital, Building 149 13th Street, Charlestown, MA 02129. E-mail: giorgio@nmr.mgh.harvard.edu

Received for publication 9 November 1999; accepted 21 June 2001

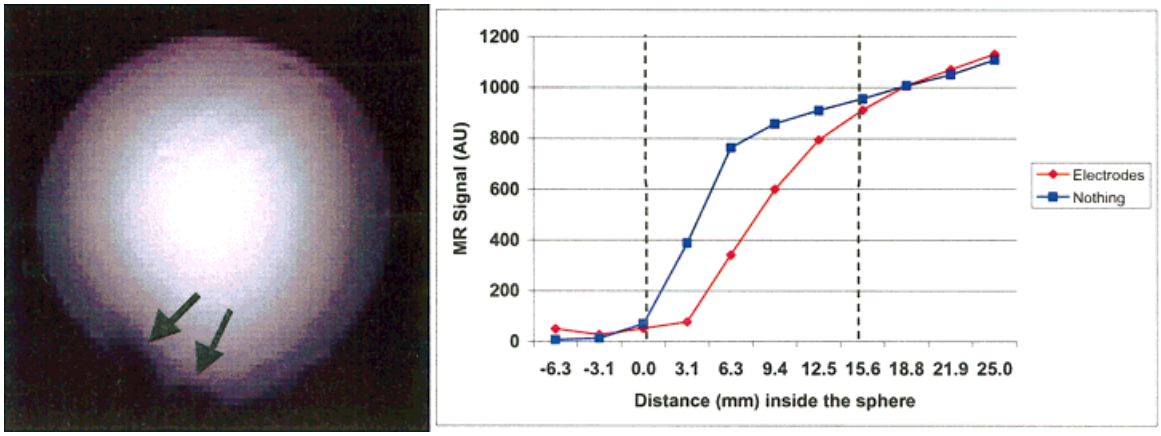

Figure 1.

Left: Gradient Echo EPI of a spherical water phantom with EEG electrodes and EEG paste (TE = 55 msec, TR = 1.1 sec, 10 slices 3 mm thick, no skip, 90° flip angle, FOV = 400 × 200 mm, matrix size 128 × 64, General Electric 3 T scanner). Signal loss is due to the presence of plastic conductive electrodes and paste (Elefix, Nihon Kohden). These areas (indicated by black arrows) demonstrate the interruption of the spherical symmetry of the water phantom. **Right:** The signal loss extends typically for 15 mm from the external plastic shell of the phantom. The partial volume effect shapes the image intensity differently from the ideal step function.

EEG recordings and to create a small magnetic susceptibility difference between the electrodes and the adjacent tissue.

Image artifacts (Fig. 1) are still present when using plastic conductive electrodes and EEG paste. For a spherical water phantom the average depth of the image artifacts are approximately 15 mm. In theory, the image artifacts should not extend to the cortical tissues given that the layers composed of skin, bone, CSF and dura are normally thicker than 15 mm. A phantom measurement alone, however, is insufficient to demonstrate that the presence of EEG electrodes and paste does not influence the BOLD signal on a human subject. Chemical shift artifacts of the fat-water interface are created when the water-based EEG gel is applied to the skin that is superficial to the adventitious fat layer.

The T2*-weighted images are inadequate to show unambiguously the presence of a signal drop on a human subject (Fig. 2) given the complex and convoluted nature of the human cortex. Furthermore, it is nearly impossible to obtain the exact same registration when comparing MRI images done with and without electrodes on the same subject because the subject is removed for placement of the EEG cap. In this study, we propose a solution to these problems by directly comparing cortical surface maps rather than trying to match up volumetric imaging measurements. In particular, we performed a retinotopic mapping study [Sereno et al., 1995] to examine the influence of the EEG electrodes or EEG paste on specifically the BOLD fMRI signal. The cortical surface map of the visual cortex was selected because the 64-channel EEG cap designed and built in our laboratory [Bonmassar et al., 1999] has the highest spatial sampling (i.e., the density of the electrodes) along the occipital lobe. The identical visual stimulation and flattening representation was used to obtain the subject's retinotopic map both with and without the electrodes in place.

The method presented in this study can easily be extended to examine the influence of EEG equipment on the BOLD fMRI signal of other cortical areas besides the visual by representing the activation of the brain region of interest on a flattened cortical surface. Examples of such representations have been shown in the following cortical regions: a) somatosensory areas [Moore et al., 2000]; b) auditory areas [Talavage et al., 2000]; c) semantic processing areas [Dale et al., 2000] (showing activation from occipital visual cortex to temporal, parietal, and frontal areas); and d) face-selective areas [Halgren et al., 1999].

MATERIALS AND METHODS

MRI acquisition

Experimental details are similar to those introduced elsewhere [Hadjikhani et al., 1998; Sereno et al., 1995] except for the modifications described below. Informed written consent was obtained from each subject before each scanning session, and the Massachusetts General Hospital Subcommittee on Human Subjects approved all procedures. Three normal human subjects with (or corrected to) normal vision were

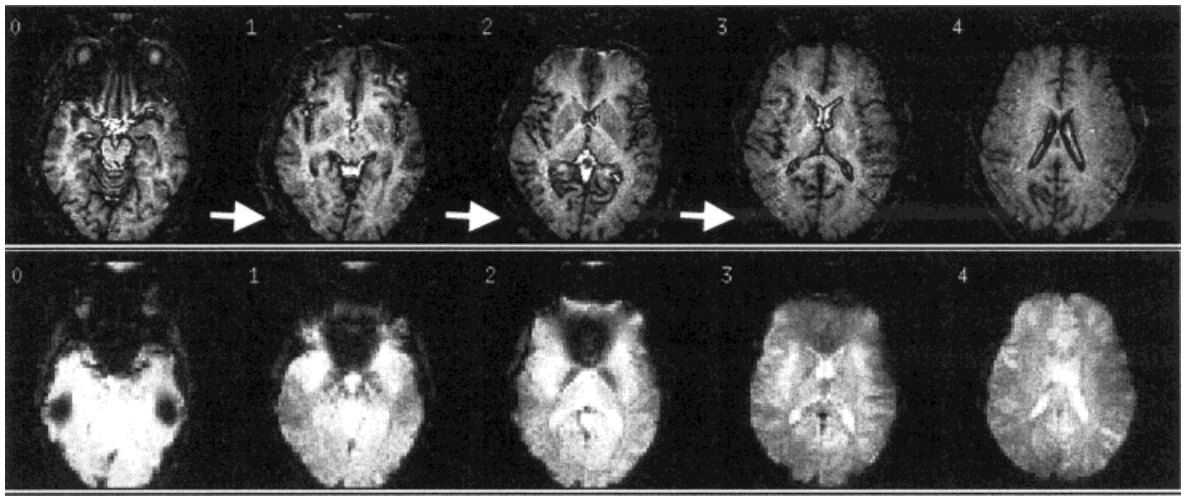

Figure 2.

T1 (top) and T2*(bottom) weighted images of a human head with EEG electrodes (conductive plastic) and EEG paste (Elefix, Nihon Kohden). **Top:** EPI high resolution T1 weighted images (EPI spin echo sequence with TE = 70 msec, TR = 12,000 msec, TI = 1,200 msec, 5 slices 4 mm thick, no skip, 90° flip angle, 3 T). The presence of the electrodes can be clearly seen on the structural images (see white arrows), and this image artifact can be used in principle to landmark the position of the EEG electrodes. **Bottom:** Functional MRI (EPI gradient echo sequence with TE = 40 msec, TR = 998 msec, 3 T) of the same subject and slice prescription in the top figure.

scanned using a 3 Tesla (T) General Electric MRI scanner retrofitted with ANMR echo-planar imaging (EPI) capability. The standard head coil was used to collect high-resolution anatomic images used in image registration and reconstruction of the cortical surface [Fischl et al., 1999]. We used a 180-mm diameter transmit/receive surface coil that covered the entire occipital pole for functional data collection. High resolution T1 EPI images were also acquired using this surface coil. Head motion was minimized using an individually molded dental impression bite bar.

T2* measurements of two different conductive EEG creams were performed to investigate the possible contribution of magnetic susceptibility. These measurements were done using a conventional gradient echo sequence (TR = 50 msec, FOV = 200 × 200 mm, matrix size 256 × 256, 1 slice, 1 mm thick, 90° flip angle, 4 averages, General Electric 1.5 T scanner) at increasing echo delays times (TE).

MR spectroscopy (MRS) data were acquired on a General Electric 1.5 T scanner using the PRESS sequence (TE = 144 msec, TR = 1.3 sec) [Bottomley, 1987]. The ROI selected was a $20 \times 20 \times 20$ mm^3 voxel and 32 averages were acquired for each spectrum.

Retinotopic mapping

Stimuli for retinotopic mapping of eccentricity [Engel et al., 1994; Hadjikhani et al., 1998; Sereno et al., 1995) were slowly expanding thin rings made of flickering arcs with random color distribution generated using a Silicon Graphics O_2 workstation with GL graphics library functions. The thin rings were segmented in 20 randomly colored sectors alternating at 4 Hz flickering frequency. Visual stimuli were rear-projected onto an acrylic screen (DaTex, Da-Lite Corp.) during fMRI scanning providing a visual field of 40° × 25° (175 × 130 mm). The screen was positioned inside the magnet immediately below the subject's jaw. A large adjustable mirror was interposed between and oriented approximately 45° to the screen and the subject's line of sight. Thus, subjects looked directly and comfortably upwards to see an image positioned on a screen at neck level. Stimuli were projected onto the screen by a Sharp 2000 color LCD projector through a collimating lens (Buhl Optical). Subjects were instructed to stare at a central fixation spot during all functional scans. Three fMRI scans of 8 min 32 sec duration were collected and averaged. Each scan covered an entire period of expansion/contraction of the ring. We used a gradient echo EPI (TR = 4 sec, TE = 30 msec, 90° flip angle, matrix 128 × 64, 1.5 × 1.5 mm in plane resolution) imaging sequence. Each scan included a total of 128 functional images per slice (i.e., time series points). Sixteen slices including all of occipital, posterior parietal and temporal lobes were acquired contiguously using 4-mm thick slices oriented perpendicular to the calcarine sulcus and extending

posteriorly to the occipital lobe. Linear detrending and baseline removal of the data was done voxel-wise by subtracting a line fitted by least squares. The time series of each pixel was subsequently analyzed using the Fast Fourier Transform (FFT). Retinotopically organized regions exhibited two peaks in the magnitude plane of the complex FFT representation corresponding to the expansion/contraction frequency (≅0.015 Hz). The phase of the FFT at this expansion/contraction frequency for every voxel of the slice is proportional to the eccentricity of the stimulus. A systematic variation of ring sizes activates different regions of the visual cortex with different time-delays or phases at the expansion/contraction frequency. All the phases were corrected considering the various delays in which the various slices were acquired. Finally, phase angles for each voxel were converted into hue values with intensity proportional to the ratio between the peak amplitude at the expansion/contraction frequency and the average of the amplitude at all other frequencies. Color-coded retinotopic data are displayed in cortical surface coordinates [Fischl et al., 1999] and resampled from a 3×3 mm^2 square cortical grid to a 1×1 mm^2 grid using linear interpolation producing a smooth representation overlaid on the subject's anatomical data. Retinotopic eccentricity maps were collected from three different subjects using three different conditions: test-retest, test-retest with poor fixation, and electrodes vs. no electrodes. The test-retest with poor fixation was a control condition and the subject was instructed not to stare continuously at the fixation point (as required for the other conditions), but to briefly and randomly loose fixation in every expansion/contraction cycle.

Matched filtering

The eccentricity maps collected were used as input to a *phase-only matched filter* [Horner and Gianino, 1984] to quantify the similarity between the maps obtained in all of our experiments. This filter has a sharp correlation peak, few sidelobes, and it is easy to implement [Yaroslavsky, 1992]. The maximum amplitude of this filter's output has been shown to provide an excellent matching index [Horner and Gianino, 1984].

Given two images $I_1(x,y)$ and $I_2(x,y)$, the Fourier transform $\mathcal{T}\{\ \}$ of these images can be written as:

$$\begin{cases} Z_1(k, h) = \mathcal{T}\{I_1(x, y)\} = X_1(k, h) + jY_1(k, h) \\ Z_2(k, h) = \mathcal{T}\{I_2(x, y)\} = X_2(k, h) + jY_2(k, h) \end{cases} \quad (1)$$

If one uses the symbol $\mathcal{T}^{-1}\{\ \}$ for the inverse Fourier Transform, the phase-only filter is given by:

$$F(x, y) = \mathcal{T}^{-1}\left\{\exp\left[j \cdot \arctan\left(\frac{X_1Y_2 - X_2Y_1}{X_1X_2 + Y_1Y_2}\right)\right]\right\} \quad (2)$$

This filter is very sensitive to edges of the eccentricity map borders (i.e., anatomical patches, see Fig. 3), and it requires for every subject a rectangular (e.g., a 150×300 pixels-image was adopted in this study) region of interest (ROI) filled with active voxels. The ROIs were aligned for comparison according to anatomical landmarks and functional images were coregistered to the corresponding structural scans. The registration is done manually by overlapping, using shift, rotation and dilation commands, a high-resolution T1 EPI volume (i.e., coregistered to the functional data) to the high resolution three-dimensional anatomic data set.

EEG cap

The fMRI data were collected with and without our 64-channel recording cap that was custom built [Bonmassar et al., 1999] in our laboratory. This non-magnetic nylon mesh cap utilizes conductive-plastic electrodes to measure the EEG or EP. The thin silver epoxy layer of the electrodes helped to decrease the contact resistance to typically 5kΩ.

RESULTS

We first investigated the MR properties of two commonly used electrode pastes. The first cream was a conductive gel (Quick-gel, Neuromedical supplies) and the second cream was an EEG paste (Elefix, Nihon Kohden). The two different formulations of the conductive creams lead to different MRI transverse signal dephasing. The EEG paste had a shorter T2* (25.6 msec) than the conductive gel (42.2 msec). In comparison, the T2* of brain tissue is approximately 50 msec for the visual cortex at 1.5 T. A combination of chemical shift and magnetic susceptibility are the expected mechanisms for the signal drop visible in the voxels adjacent to the paste (not shown). For EEG electrodes along with EEG paste, however, magnetic susceptibility effects are most likely the dominant dephasing mechanism.

MRS and T2*measurements were performed on these two different samples of EEG creams to investigate the possible contribution of chemical shift artifacts. The first cream tested was "Quick-gel" (Neuro-

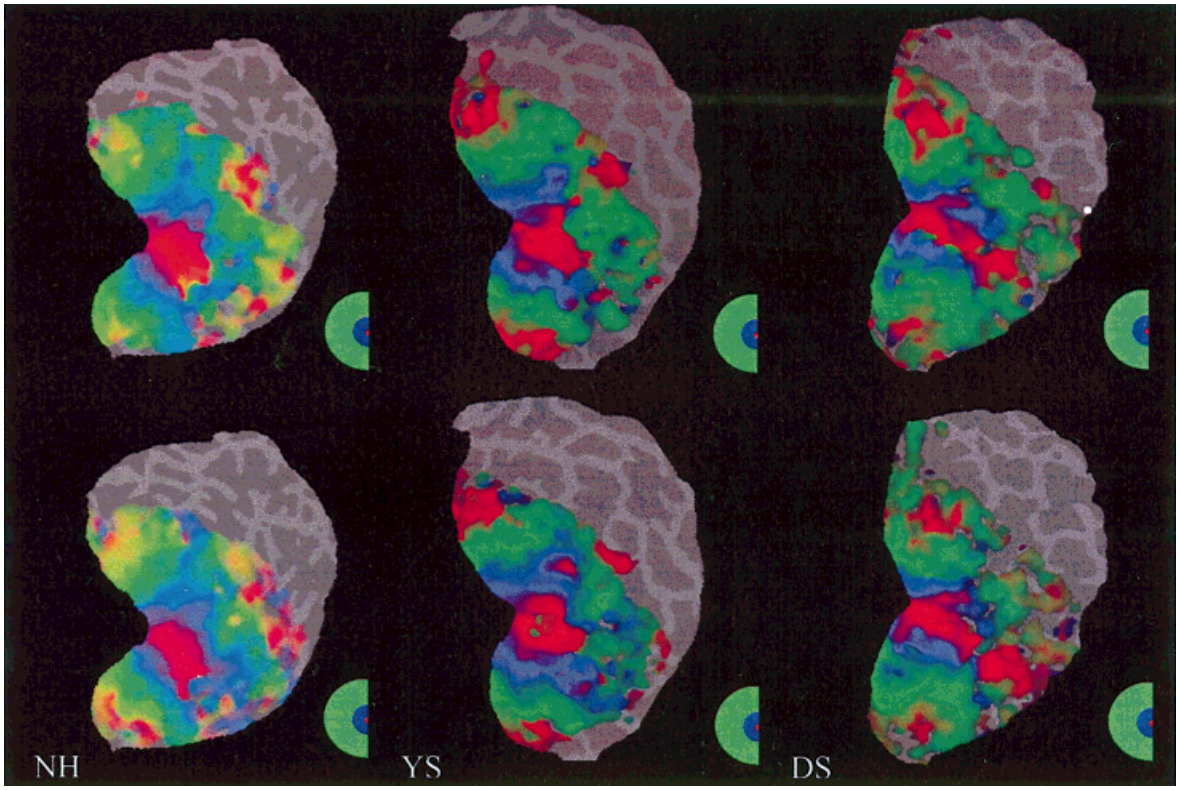

Figure 3.

Retinotopic maps with/without EEG electrodes. The top row shows the retinotopic maps of the right visual hemifield in three different subjects (NH, YS and DS). Subsequently, 64 EEG electrodes were then placed on the subjects' head. The bottom row shows the retinotopic maps (right visual hemifield) of the same subjects wearing the EEG cap within the 3 T magnet. The small differences between the two-retinotopic maps are due to normal physiological variations.

medical supplies) and exhibited a very broad water peak. The second cream tested was "Elefix" (Nihon Kohden) and exhibited two spectral peaks of water and fat (the later, presumably due to the oil content of the EEG paste). The ratio between the two amplitudes of the water/oil peaks was 135/170 indicating a high concentration of oil in the "Elefix" cream.

From the spectroscopy and the T2* study we conclude that the water based gel ("Quickgel") is preferable to the oil based paste. The T2* time constant of the gel is closer to the one of the brain, hence creating a smaller magnetic susceptibility at the interface. The absence of a fat peak in the gel enables the use of conventional fat-suppression sequences to correct for the chemical shift image artifact of the adventitious skin-fat layer.

Using the phase-encoded retinotopic mapping procedure, we determined whether the presence of both electrodes and conductive gel actually affects the measured fMRI BOLD response. Figure 3 shows the individual (n = 3) retinotopic maps, with and without the electrodes in place. Qualitatively, the maps appear quite similar. Figure 4 shows the corresponding average response of the phase-only matched filter to the left and right hemifields. The shape of the filter's output resembles closely a delta function, indicating that the filter has found a good match between the retinotopic maps of these three subjects wearing the EEG cap. These results demonstrate that the EEG electrodes and gel do not significantly perturb the fMRI measurements. Figure 5 shows the average response of the filter to the left and right hemifields, for a test-retest and for a control condition. The plot of the control condition is clearly very noisy, and the filter easily reveals the poor match of the retinotopic maps (not shown) due to the subject's lack of fixation. Figures 4 and 5 demonstrate similar variability for both the electrodes/no electrodes and the test-retest conditions.

Table I presents the proposed index or the amplitude of the maximum peak (MP) of the phase-only filter (POF) and its location. A small MP amplitude, ~15 dB attenuation with respect to the ideal upper bound of the MP (i.e., phase only autocorrelation or

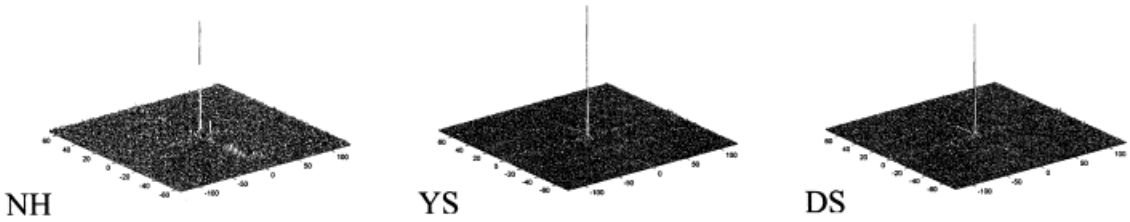

Figure 4.
Output of the Phase-Only Filter for the retinotopic maps with/without EEG electrodes (Fig. 3). The x and y-axis are pixel indices with the origin in the center, and the z-axis is expressed in arbitrary units.

POA, MP = 1), and an MP position other than the origin are clear indications of a poor match (last column). The MP values in the first two columns are excellent matches [Vijaya Kumar and Hassebrook, 1990]. In practice, one can assume that phase-only correlation peaks of approximately 0.5 or greater can be considered adequate for simultaneous EEG/fMRI measurements.

DISCUSSION

Our current approach in simultaneous EEG/fMRI measurements is to increase the number of electrodes to improve EEG source localization [Liu, 2000]. Furthermore, an increased number of electrodes can improve the SNR of the EEG recordings that are affected by Faraday's currents (i.e., ballistocardiogram noise) induced by physiological and microscopic movements of the subject inside a strong magnetic field [Huang-Hellinger et al., 1995]. Notably, a larger number of electrodes allows one to more effectively apply a spatial filter [Bonmassar et al., 1999, 2001; Schomer et al., 2000] due to the fact that the ballistocardiogram noise is rather uniformly sensed at all of the electrodes. Thus, a larger array of electrodes provides a better sampling grid for spatial filtering. The presence of an increasing number of EEG electrodes and paste inside the FOV can potentially be detrimental to simultaneous EEG/fMRI recordings. Understanding these issues plays an important role in preserving the original signal quality of fMRI in simultaneous EEG/fMRI recordings. Further work is required to determine the tradeoff between image sensitivity and spatial selectivity inherent to fMRI (e.g., at higher magnetic fields) as well as EEG recording quality.

Using our experimental setup we have tested a 64-channel cap and have observed that the MRI signal in proximity to EEG electrodes exhibits an intensity drop (Figs. 1, 2) very likely due to magnetic susceptibility but with a maximum depth typically of less than 15 mm. In principal, this type of artifact on the high-resolution T1 images can be used to landmark the position of the EEG electrodes on the surface of the subject head. Despite the ability to register the electrodes no adverse effect on the fMRI images was observed due to the presence of EEG electrodes and paste (Figs. 3, 4).

Most of the existing fMRI data has been collected using gradient echo (GE) sequences [Bandettini et al., 1992; Belliveau et al., 1991; Blamire et al., 1992; Frahm et al., 1992; Kwong et al., 1992; Ogawa et al., 1992; Turner et al., 1993]. This technique, however, is very

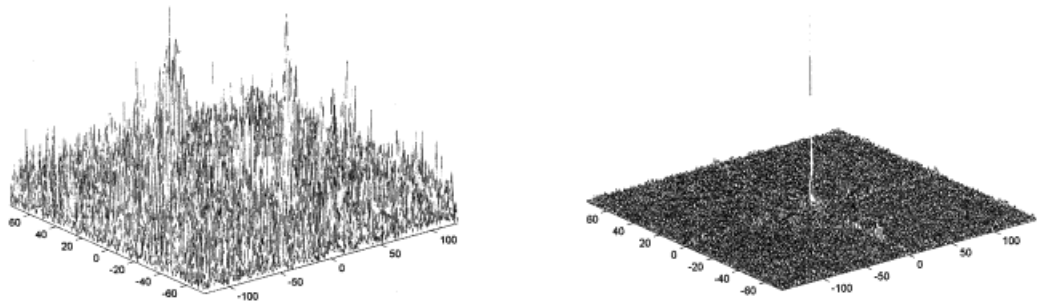

Figure 5.
Output of the Phase-Only Filter for the retinotopic mapping of poor fixation condition (left) and test-retest (right). The x and y-axis are pixel indices with the origin in the center, and the z-axis is expressed in arbitrary units.

TABLE I. Numerical results showing the matched filter's discrimination capabilities

	Test-retest	Electrodes vs. no electrodes	Control: test-retest poor fixation
Maximum peak	0.46	0.48/0.46/0.68	0.0350
Peak location	(0,0) Fig. 5	(0,0)/(0.0)/(0.0) Fig. 4	(−2,50) Fig. 5

sensitive to magnetic susceptibility changes. The asymmetric spin echo sequence (ASE) is more immune to arterial large-scale susceptibility artifacts and more sensitized to capillary level susceptibility effects [Fisel et al., 1991]. Unfortunately, the greater RF power dissipation of the ASE exposes the subject to a greater risk of temperature increase [Lemieux et al., 1997; Schaefer, 1992]. Thus, in practice, both at 3 T and 1.5T we use a GE sequence.

The present study was performed using a custom-built surface coil shaped to fit the posterior portion of the head. No adverse influence on our imaging system has ever been observed using our experimental setup during simultaneous EEG/fMRI. The previous data utilized a transmit/receive (T/R) surface coil. When using a quadrature birdcage T/R head coil [Collins et al., 1998] the presence of EEG electrodes affects the tuning and the Q-factor contour lines of the coil. The loss in RF signal caused by this interference can be reduced by running the EEG cables from the subject's head to the amplifiers along the axis of the head coil.

CONCLUSION

In the present study, we have introduced a matched-filtering method to estimate the influence of EEG electrodes, leads, and paste on specifically the BOLD fMRI signal. The filter's output peak intensity was used as an index to quantify the quality of the fMRI signal during simultaneous EEG recordings. The proposed index can be easily extended to other types of simultaneous measurements (e.g., optical imaging, infrared imaging, transcranial magnetic stimulation, ultrasound imaging, etc.) where the influence of various instruments or materials on the fMRI signals need to be assessed. One of the most appealing features of the method is its insensitivity to different slice prescriptions that are normally taken during scanning when inserting a subject multiple times inside a MRI scanner. Our results (see Table I) indicate that there is an excellent match between retinotopic maps with or without the presence of our custom built 64-channel EEG cap for simultaneous EEG/fMRI recordings.

ACKNOWLEDGMENTS

The authors wish to thank the reviewers for suggesting improvements to the manuscript. The authors also wish to acknowledge Anders Dale, Bruce Fischl, Leo Garrido, Bruce Jenkins, Ken Kwong, and Tim Reese for very helpful discussions and comments. This study was supported by grants from the Whitaker Foundation, United States Public Health Service NIH RO1 NS37462, P41 RR14075, the National Foundation for Functional Brain Imaging, and conducted during the tenure of an Established Investigatorship from the American Heart Association to J.W.B.

REFERENCES

Bandettini PA, Wong EC, Hinks RS, Tikofsky RS, Hyde JS (1992): Time course EPI of human brain function during task activation. Magn Reson Med 25:390–397.

Belliveau JW, Kennedy DN, McKinstry RC, Buchbinder BR, Weisskoff RM, Cohen MS, Vevea JM, Brady TJ, Rosen BR (1991): Functional mapping of the human visual cortex by magnetic resonance imaging. Science 254:716–719.

Blamire AM, Ogawa S, Ugurbil K, Rothman D, McCarthy G, Ellermann JM, Hyder F, Rattner Z, Shulman RG (1992): Dynamic mapping of the human visual cortex by high-speed magnetic resonance imaging. Proc Natl Acad Sci USA 89:11069–11073.

Bonmassar G, Anami K, Ives J, Belliveau JW (1999): Visual evoked potential (VEP) measured by simultaneous 64-Channel EEG and 3T fMRI. NeuroReport 10:1893–1897.

Bonmassar G, Schwartz DP, Liu AK, Kwong KK, Dale AM, Belliveau JW (2001): Spatiotemporal brain imaging of visual-evoked activity using interleaved EEG and fMRI recordings. NeuroImage 13:1035–1043.

Bottomley P (1987): Spatial localization in NMR spectroscopy in vivo. Ann NY Acad Sci 508:333–348.

Chiappa K, Hill R, Huang-Hellinger F, Jenkins B (1999): Photosensitive epilepsy studied by functional magnetic resonance imaging and magnetic resonance spectroscopy. Epilepsia 40:3–7.

Collins CM, Li S, Smith MB (1998): SAR and B1 field distributions in a heterogeneous human head model within a birdcage coil. Magn Reson Med 40:847–856.

Dale A, Liu A, Fischl B, Buckner R, Belliveau J, Lewine J, Halgren E (2000): Dynamic statistical parametric mapping: combining fMRI and MEG for high-resolution imaging of cortical activity. Neuron 26:55–67.

Engel SA, Rumelhart DE, Wandell BA, Lee AT, Glover GH, Chichilnisky EJ, Shadlen MN. (1994): fMRI of human visual cortex. Nature 369:525.

Fischl B, Sereno MI, Dale AM (1999): Cortical surface-based analysis. II: Inflation, flattening, and a surface-based coordinate system. Neuroimage 9:195–207.

Fisel CR, Ackerman JL, Buxton RB, Garrido L, Belliveau JW, Rosen BR, Brady TJ (1991): MR contrast due to microscopically heterogeneous magnetic susceptibility: numerical simulations and

applications to cerebral physiology. Magn Reson Med 17:336–347.

Frahm J, Bruhn H, Merboldt K-D, Hanicke W (1992): Dynamic MRI of human brain oxygenation during rest and photic stimulation. J Magn Reson Imaging 2:501–505.

Hadjikhani N, Liu AK, Dale AM, Cavanagh P, Tootell RB (1998): Retinotopy and color sensitivity in human visual cortical area V8. Nat Neurosci 1:235–240.

Halgren E, Dale A, Sereno M, Tootell R, Marinkovic K, Rosen B (1999): Location of human face-selective cortex with respect to retinotopic areas. Hum Brain Mapp 7:29–37.

Hill R, Chiappa K, Huang-Hellinger F, Jenkins B (1999): Hemodynamic and metabolic aspects of photosensitive epilepsy revealed by functional magnetic resonance imaging and magnetic resonance spectroscopy. Epilepsia 40:912–920.

Horner JL, Gianino PD (1984): Phase-only matched filter. Applied Optics 23:812–816.

Huang-Hellinger FR, Breiter HC, Mc Cormack G, Cohen MS, Kwong KK, Sutton JP, Savoy RL, Weisskoff RM, Davis TL, Baker JR, Belliveau JW, Rosen BR (1995): Simultaneous functional magnetic resonance imaging and electrophysiological recording. Hum Brain Mapp 3:13–23.

Ives JR, Keenan JP, Schomer DL, Pascual-Leone A (1998): EEG recording during repetitive transcranial magnetic stimulation (rTMS). Neurology 4(Suppl):A167.

Ives JR, Warach S, Schmitt F, Edelman RR, Schomer DL (1993): Monitoring the patient's EEG during echo-planar MRI. Electroenceph Clin Neurophysiol 87:417–420.

Krakow K, Allen P, Symms M, Lemieux L, Josephs O, Fish D (2000): EEG recording during fMRI experiments: image quality. Hum Brain Mapp 10:10–15.

Krakow K, Wieshman UC, Woermann FD, Symms MR, McLean MA, Lemieux L, Allen PJ, Barker GJ, Fish DR, Duncan JS (1999): Multimodal MR imaging: functional, diffusion tensor, and chemical shift imaging in a patient with localization-related epilepsy. Epilepsia 40:1459–1462.

Lemieux L, Allen JP, Franconi F, Symms MR, Fish DR (1997): Recording of EEG during fMRI experiments: patient safety. Magn Reson Med 38:943–952.

Liu A (2000): Spatiotemporal brain imaging. Ph.D. Thesis: Massachusetts Institute of Technology.

Lufkin R, Jordan S, Lylyck P, Vinuela F (1988): MR imaging with topographic EEG electrodes in place. Am J Neuroradiology 9:953–954.

Moore C, Chantal E, Corkin S, Fischl B, Gray A, Rosen B, Dale A (2000): Segregation of somatosensory activation in the human Rolandic cortex using fMRI. J Neurophysiol 84:558–569.

New PFJ, Rosen BR, Brady TJ, Buonanno FS, Kistler JP, Burt CT, Hinshaw WS, Newhouse JH, Pohost GM, Taveras JM (1983): Potential hazards and artifacts of ferromagnetic and nonferromagnetic surgical and dental materials and devices in NMR imaging. Radiology 147:139–148.

Ogawa S, Tank DW, Menon R, Ellermann JM, Kim S-G, Merkle H, Ugurbil K (1992): Intrinsic signal changes accompanying sensory stimulation: functional brain mapping with magnetic resonance imaging. Proc Natl Acad Sci USA 89:5951–5955.

Schaefer DJ (1992): Dosimetry and effects of MR exposure to RF and switched magnetic fields. Ann NY Acad Sci 649:225–236.

Schomer LD, Bonmassar G, Seeck M, Lazeyras F, Blum A, Anami K, Schwartz D, Belliveau JW, Ives J (2000): EEG linked functional magnetic resonance imaging in epilepsy and cognitive neurophysiology. J Clin Neurophysiol 17:43–58.

Seeck M, Lazeyras F, Michel CM, Blamke O, Gericke CA, Ives J, Delavelle J, Golay X, Haenggeli CA, De Tribolet N, Landis T (1998): Non-invasive epileptic focus localization using EEG-triggered functional MRI and electromagnetic tomography. Electroenceph Clin Neurophysiol 106:508–512.

Sereno MI, Dale AM, Reppas JB, Kwong KK, Belliveau JW, Brady TJ, Rosen BR, Tootell RBH (1995): Borders of multiple visual areas in humans revealed by functional magnetic resonance imaging. Science 268:889–893.

Symms MR, Allen PJ, Duncan JS (1999): Reproducible localization of interictal epileptiform discharges using EEG-triggered fMRI. Phys Med Biol 44:N161.

Talavage TM, Ledden PJ, Benson RR, Rosen BR, Melcher JR (2000): Frequency-dependent responses exhibited by multiple regions in human auditory cortex. Hear Res 150:225–244.

Turner R, Jezzard P, Wen H, Kwong KK, Le Bihan D, Zeffiro T, Balaban R (1993): Functional mapping of the human visual cortex at 4 and 1.5 Tesla using deoxygenation contrast EPI. Magn Reson Med 29:277–279.

Vijaya Kumar B, Hassebrook L (1990): Performance measure for correlation filters. Applied Optics 29:2997–3006.

Warach S, Ives JR, Schlaug G, Patel MR, Darby DG, Thangaraj V, Edelman RR, Schomer DL (1996): EEG-triggered echo-planar functional MRI in epilepsy. Neurology 47:89–93.

Yaroslavsky L (1992): Is the phase-only filter and its modifications optimal in terms of the discrimination capability in pattern recognition? Applied Optics 31:1677–1679.